Exhibit F - UTCRS

UTC Project Information	
Project Title	Ultrasonic Tomography for Infrastructure Inspection
University	Texas A&M University (TAMU)
Principal Investigator	Stefan Hurlebaus, Ph.D., Civil Engineering (PI)
PI Contact Information	3135 TAMU College Station, TX 77843-3135 Office (979) 845-9570 shurlebaus@tamu.edu
Funding Source(s) and Amounts Provided (by each agency or organization)	Federal Funds (USDOT UTC Program): $104,653 Cost Share Funds (TAMU): $54,909
Total Project Cost	$159,562
Agency ID or Contract Number	DTRT13-G-UTC59
Start and End Dates	January 2014 – December 2016
Brief Description of Research Project	The structural integrity of railroad infrastructure is critical in order to address structural repair needs in a timely fashion and ensure rail safety. This includes the regular inspection and maintenance of railroad tunnel linings and timber beams and ties. Since tunnels are naturally in an aggressive environment that is not conducive to lane closures, early detection that leads to preventive maintenance is a necessity. The occurrence of damage and deterioration in railroad timber beams and ties can lead to failure of the components and, in the worst case, derailment of the train. According to the Federal Railroad Administration (FRA), wide gages due to defective/missing crossties accounted for the highest percentage (17.1%) of all railway accidents in the US from 2008-2011 (FRA, 2011). It is, therefore, crucial to detect damage at an early stage so that, by taking appropriate measures, failure can be prevented. The proposed project will examine the use of Ultrasonic Tomography (UST) to examine the interior of wooden beams and crossties as well as railroad tunnel linings on-site. The Ultrasonic Tomographer employs

	a matrix (4x12) of low-frequency, shear transducers that generate shear waves through the depth of a specimen under test. The waves are reflected by internal discontinuities and changes in medium (such as concrete, air, and steel). This behavior is utilized to map voids, delamination, cracks, and other defects, as well as structural depth and reinforcement presence. The waves are sequentially emitted and received by 66 paired transducers per single scan, causing repeated reflections and patterns to stand out for inspection. Through the use of dry-point-contact piezoelectric sensors, the transducers do not require the use of a coupling agent, making it practical for on-site applications. The recorded signals undergo automated signal processing to identify the existence, location, and size of the potential discontinuities. The UST technique can be used to map entire 3D images of concrete sections as well as single-point evaluations.
Describe Implementation of Research Outcomes	**INTRODUCTION** The Synthetic Aperture Focusing Technique (SAFT) algorithm is a post-processing algorithm that converts reflected ultrasonic data into a high-resolution image. The first one-dimensional implementation of the SAFT algorithm was in the late 1970s, following the wide use of radar technology. For smaller transducers at lower frequencies, the SAFT algorithm performs with higher accuracy when compared to other imaging techniques (Dengzhi, 2007). In 1982, Pacific Northwest Laboratory conducted studies to incorporate the SAFT algorithm in field equipment, following extensive research conducted by Hall et al. (1986). It is important to note that the basic theory for the SAFT algorithm is only applicable to homogeneous materials, but it can be modified in order to accurately work for non-homogenous materials like reinforced concrete. The SAFT algorithm creates high-resolution images by superimposing several pulse echo signals that have been measured at various positions (Kotoky and Shekhar, 2013). The linear SAFT algorithm aides in the clarity of the images by numerically superimposing the data transmitted and received by the array of dry contact transducers. SAFT creates images based on results from either B- or C-scans, series of received signal that are perpendicular and parallel to the surface, while filtering out scattering. This leads to a clear and more precise image that can accurately depict the defects (Burr et al., 1998).

To minimize attenuation, transducers using low frequencies between 30 and 80 kHz are typically used for the inspection of concrete (Kotoky and Shekhar, 2013). For reinforced concrete, which has nonhomogeneous property causing noise, minimizing the structural noise is critical because it can disguise some defects and inaccurately display others.

Most commercial SAFT algorithms in nondestructive testing are inaccessible and designed for specific geometries of devices. Therefore, an in-house SAFT algorithm based on time-domain for the prototype device was developed.

GEOMETRY OF SAFT ALGORITHM

As measurements are required at various positions, it is necessary to have the device send pulse echoes in an array. Using the post-processing algorithm, engineers can translate ultrasonic data into images that can accurately identify the vast majority of defects, such as; delamination, water filled void, air voids, and honeycombing.

It is critical to know the path travelled by the ultrasonic wave from the emitting transducer to the defect and back to the receiving transducer, for SAFT to create images from the ultrasonic transmission data. Therefore, an A-scan is necessary to provide geometric guidance and restore the image. Once the receiving transducers have received all emitted signals, the algorithm superimposes this computed data, resulting in a high resolution image. A time-frequency template of the signals is used over a Fourier transform. The time-frequency analysis is based on Wigner-Ville distribution.

Kotoky and Shekhar (2013) explain that the basics of the SAFT algorithm rely on geometrical reflection of the wave. For this, the focus of the ultrasonic transducers can be assumed to be in constant phase (so, the amplitude is consistent) before diverging at various angles in a cone shape. The angle of deflection is determined by transducer properties, primarily focal length and diameter. Because of this, it is necessary for the system to use a single type of transducer, because waves propagating at various angles would make the algorithm difficult, if not impossible. The properties of the transducer can be calculated easily knowing the path length and travel time for a signal moving along that path. The aperture of the transducer, and the diameter of wave perpendicular to wave propagation, are critical

	because it assists in the layering of the A and B scan. The aperture width of the transducer corresponds to the width of the cone, and at what range it can be applied. The path length that the signal must travel corresponds to the phase shift seen in the signal. From these geometric properties, an engineer can construct images that simplify the detection of defects below the concrete surface (Kotoky and Shekhar, 2013). This geometric interpretation can be seen in Figure 1 through Figure 3.

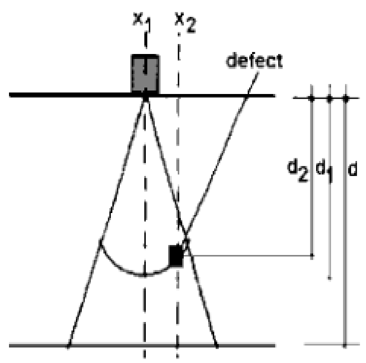

Figure 1: Display of the Waves Passing through the Defect Zone (Kotoky and Shekhar, 2013).

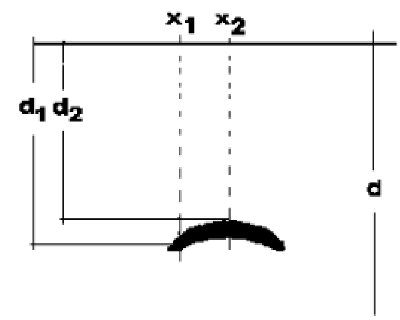

Figure 2: B-Scan of the Iron Defect (Kotoky and Shekhar, 2013).

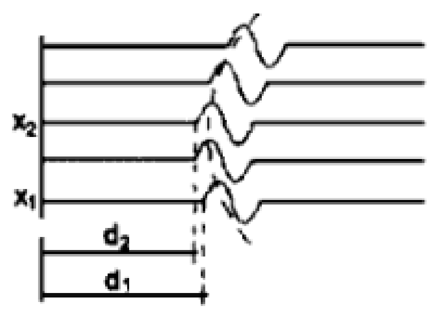

Figure 3: Resulting Image Produced from the Wave Passing Through the Defect (Kotoky and Shekhar, 2013).

As shown in Figure 1, the wave is sent from the transducer at a distance x_1 in a conical shape, interacting with the defects at x_2. When the wave interacts with the defect, which is at a depth d_2, the same wave is at a depth d_1 from the surface directly below the transducer. From this, Figure 2 can be obtained showing the shape of the waves and the various distances. This image displays the detection of a single round hole in an iron block. The final broad image is then produced using the transducer aperture width. With this technique, the A-scan

	is focused below the transducer as shown in Figure 1, which corresponds to the B-scan in Figure 2. These images are ultimately used to produce the final image in Figure 3. With SAFT, the intention is to determine a parabola at each data point where a significant amount of energy is dispersed. If the summation of energy values over this parabola at a point is high, it is marked as a scattering point. For the scattering of signal in non-homogeneous materials, it is important to know properties of this parabola, or conical shape, to reduce noise. In order to successfully reduce scattering, the parabola must be short in comparison with the whole array of transducers because of its larger size. In addition, by producing a smaller parabola, the algorithm is more efficient. Apart from relative shortness, it is important that the parabola be thick in order to average out noise due to small changes in the material. By using a thicker line, the amplitude indicating flaws is not as large, and it evens out noise for non-homogeneous material. Only a flaw with the same length or larger than the thickness of the parabola can be detected, removing all the noise present in a non-homogeneous material (Burr et al., 1998). **NONLINEAR SAFT** In the mid-1990s, it was difficult to interpret the results using the original SAFT algorithm, and it usually required a trained engineer to decipher recorded data (Burr et al., 1998). The algorithm was later modified to overcome these shortcoming. The modifications to the SAFT algorithm, previously known as a non-linear SAFT algorithm, are necessary for concrete structures which are non-homogeneous. Non-linear modification requires that the A- or B-scan of the surface be known from the linear system. **NOISE REDUCTION** Noise reduction is relatively simple in homogeneous materials when compared to non-homogeneous materials. The spectrum of displacement may be calculated from the spectrum of the signal (at a specific location and frequency) multiplied by the signal's impulse response (from passage through the structure). From deconvolution, the incident wave scattering is easy to handle in a homogeneous material, but not with a non-homogeneous material like reinforced concrete. In non-homogeneous materials, the calculated scatter does not match with under inspection that has different stiffness or the actual scattering of the signal. The SAFT algorithm can be further

modified to account for flaw lengths that are much larger than the length of the non-homogeneous particles. The correlation between two reflected signals at two different points in the transducer array may be used to differentiate between the signals from the defects and those that are related to structural noise.

BASIC THEORY OF SAFT ALGORITHM IN TIME DOMAIN

One of the main goals in developing an in-house SAFT algorithm was to devise an algorithm that will be easy to construct and implement. A time-domain SAFT algorithm was developed for this investigation. The two major assumptions that were made in this study in order to develop a SAFT algorithm were: (1) isotropic material, which means that the wave in material medium propagates at a constant speed, and (2) material homogeneity, because the prototype device has lower frequency range, which means that it has longer wave length than the size of aggregate and non-homogeneous property of reinforced concrete rarely affect the result of SAFT. So, an area density is considered to indicate an anomaly, such as a damaged region, or rebar location.

Mathematically, sectional material properties can be described using the reflectivity. The relationship between the reflectivity function, $f(x,z)$, and the A-scan data, $s(x_e, x_r, t)$, is given by

$$s(x_e, x_r, t) = \int_x \int_z f(x,z)\delta\big(t^*(t, x_e, x_r, x, z)\big)\mathrm{d}z\,\mathrm{d}x, \qquad [1]$$

where δ is the transmitted impulse, x_e and x_r are the horizontal location of emitting and receiving transducers, respectively, x and z are the horizontal and vertical position in the region of interest (ROI), respectively, t is the time, and t^* is defined as

$$t^* = t - \frac{1}{c}\left(\sqrt{z^2 + (x - x_e)^2} + \sqrt{z^2 + (x - x_r)^2}\right), \qquad [2]$$

where c denotes the wave velocity and is constant.

Predicting the exact behavior of transmitted impulse and calculating the reflectivity function using Eq. [1] is rarely possible since measured data contains noise. To overcome this difficulty, sectional image is reconstructed from the received A-scan data. The equation for the reconstructed image, $O(x,z)$, for a continuous system is described as

$$O(x,z)=\int_{x_{emin}}^{x_{emax}}\int_{x_{rmin}}^{x_{rmax}}\alpha(x_e,x_r,x,z)s\left(x_e,x_r,t_f\right)\mathrm{d}x_r\,\mathrm{d}x_e, \qquad [3]$$

where $[x_{emin}, x_{emax}]$ and $[x_{rmin}, x_{rmax}]$ is the range of emitting and receiving transducers, respectively, α is the apodization factor, and t_f is the time of flight that is given by (Figure 4),

$$t_f=\frac{1}{c}\left(\sqrt{z^2+(x-x_e)^2}+\sqrt{z^2+(x-x_r)^2}\right). \qquad [4]$$

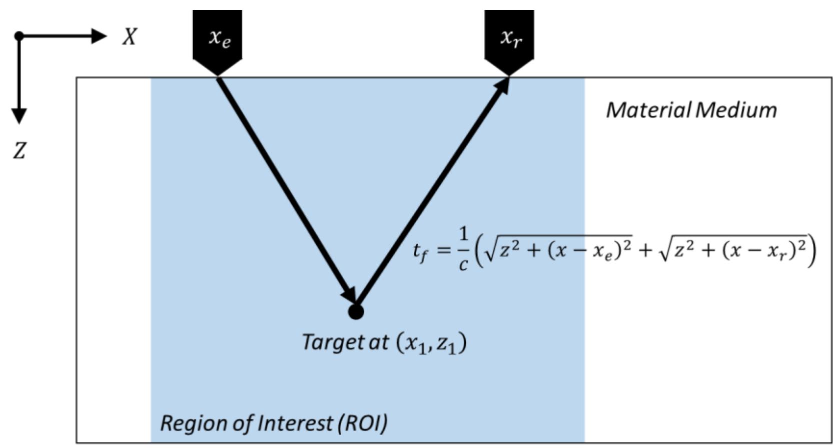

Figure 4: Geometry of Measuring Wave Propagation.

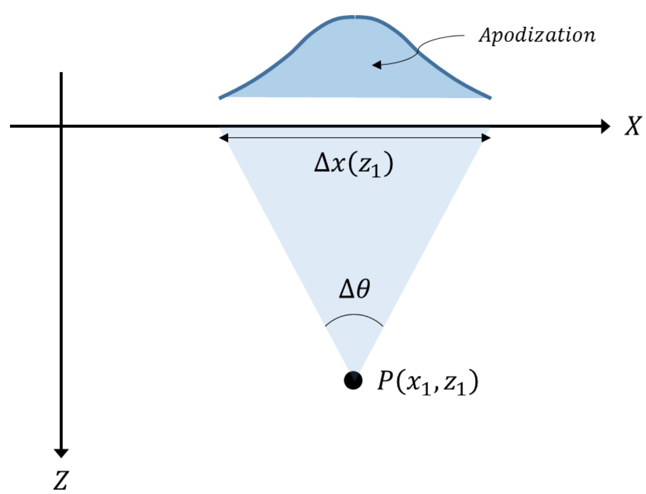

Figure 5. Illustration of Hann Function.

Apodization factor is a weighing function that reduces the effect of side lobe artifacts in the focused image. The Hann function, as shown in Figure 5, was used as an apodization function in this study. However, the transducers used in this research generate finite number of A-scan pairs. The discrete form of Eq. [3] is given as

$$O(x,z) = \sum_{e=1}^{T-1} \sum_{r=e+1}^{T} \alpha(x_e, x_r, x, z) s\big(x_e, x_r, t_f\big), \qquad [5]$$

where T is the number of sensor locations, and e and r are the indexes for the emitting and receiving transducers, respectively. Datasets with more A-scans generally have higher resolution.

VALIDATION

In order to verify the feasibility of the developed SAFT algorithm, B-scan image from the MIRA A1040 device was used. The MIRA device has 4 by 12 array of transducers and provides reconstructed B-scan images using its own embedded SAFT algorithm. The device generates a series of A-scans from the single scan. In a single scan, 1st column of transducers transmits wave impulse and 2nd to the last of arrays record wave reflections. Then, 2nd column of transducers array transmits wave impulse and 3rd to last arrays record wave reflections. This way, 66 pairs of A-scans were generated. Figure 6 shows an example of the B-scan results from the MIRA device, and the corresponding A-scan data extracted from the device. The B-scan image identifies two groups of defects located at a depth of 120 mm and 300 mm from the surface.

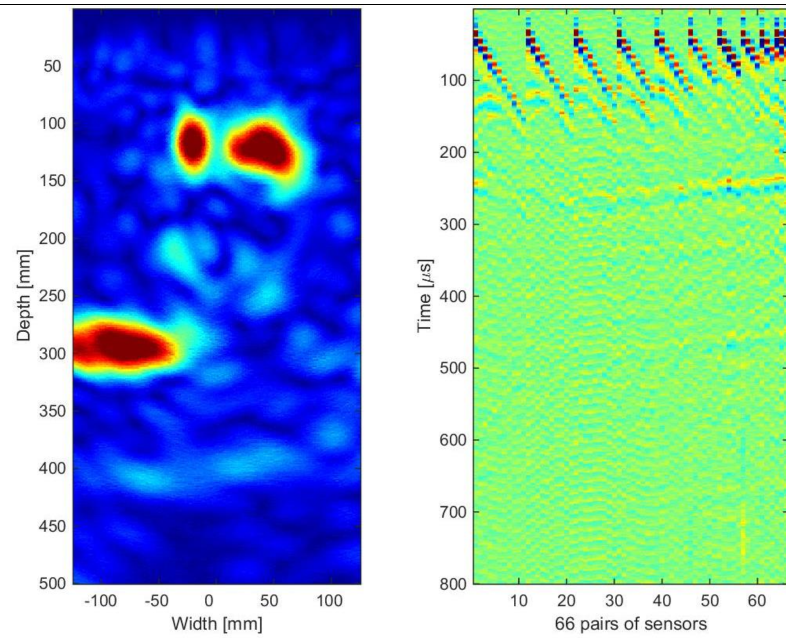

Figure 6: B-Scan Image (left), and Extracted A-Scan Data (right) from MIRA Device.

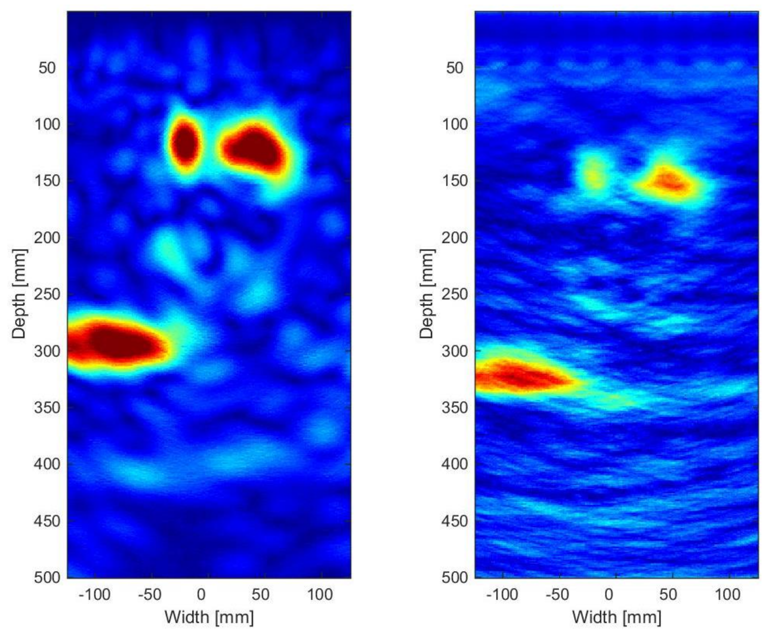

Figure 7: Comparison of B-Scan Images from the MIRA Device (left) and the developed SAFT Algorithm (right).

The A-scan data was extracted from the MIRA device and used as input data to the developed SAFT algorithm (Figure 6). Figure 7 shows a comparison of the B-scan images obtained from the MIRA device and the developed SAFT algorithm. Similar defect shapes were reconstructed in both cases. The developed algorithm generated slightly rougher image compared to the MIRA device. Both, however, are equally effective in detecting areas of high reflectivity. Additionally, the B-scan from the developed SAFT algorithm detects the defects approximately 30 mm below the defects detected in the B-scan from the MIRA device.

3D VISUALIZATION AND OTHER SECTIONAL VIEWS

The B-scans provide only sectional information, and the users may have difficulty understanding the three-dimensional distribution of defects from the two-dimensional B-scans. On the other hand, three-dimensional view of SAFT images help users to intuitively understand the location of defects relative to each other.

A three-dimensional visualization tool was developed using MATLAB. Once multiple layers of B-scan images are obtained, the reflectivity values between the layers are calculated by linear interpolation. As shown in Figure 8, points that have reflectivity above a certain value are represented in three-dimensional perspective.

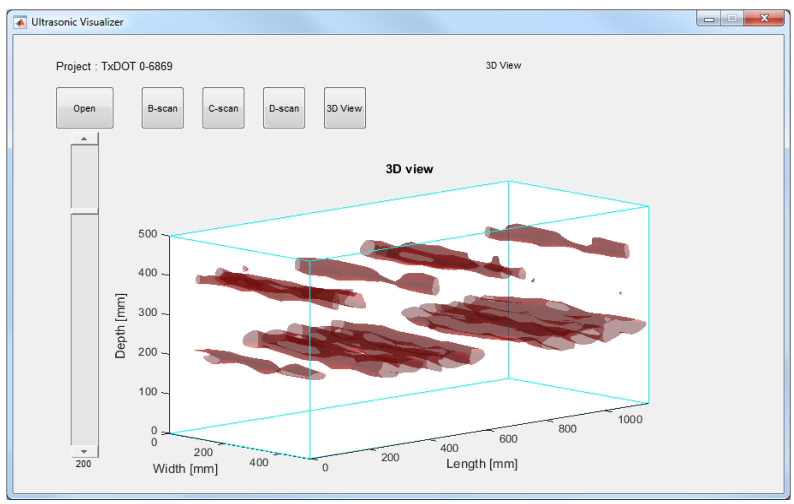

Figure 8: 3D View of Reflectivity.

The three-dimensional visualization tool allows the users to change reflectivity displayed using a slide bar. Additionally, users can also rotate the three-dimensional view. A complete section view provides the information of the entire section, so users can easily detect high reflective areas in a particular section. This visualization tool also provides sectional view functions like B-scan, C-scan, and D-scan. The B-scan of the entire section in Figure 9 is generated by combining B-

	scan images on the same plane. C- and D-scans of the entire section shown in Figure 10 and Figure 11, respectively, are extracted from three-dimensional reflectivity. 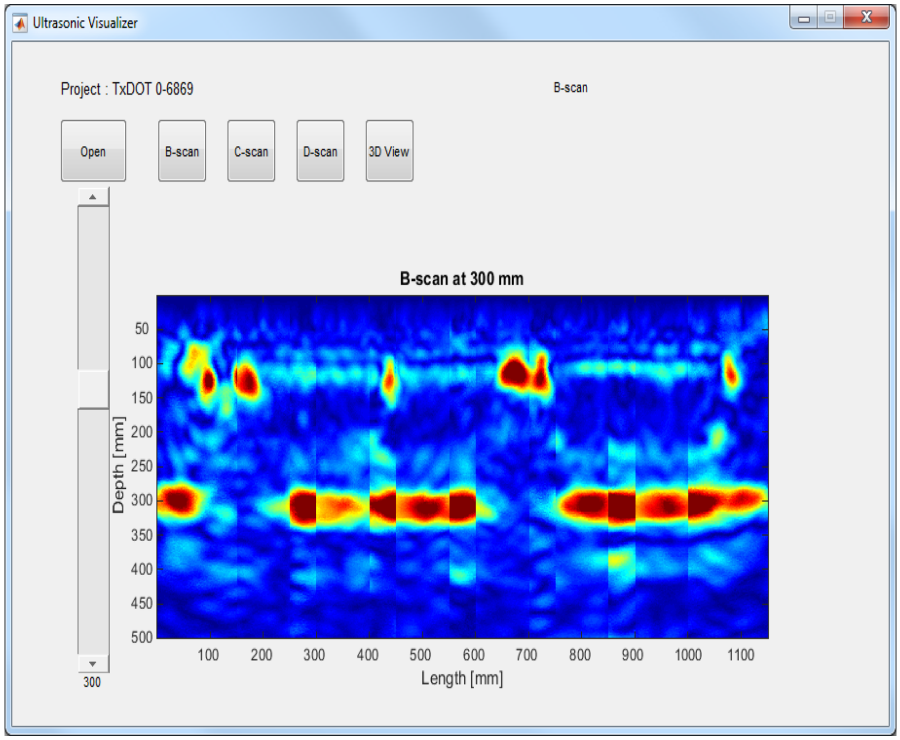 Figure 9: B-Scan of Complete Section. 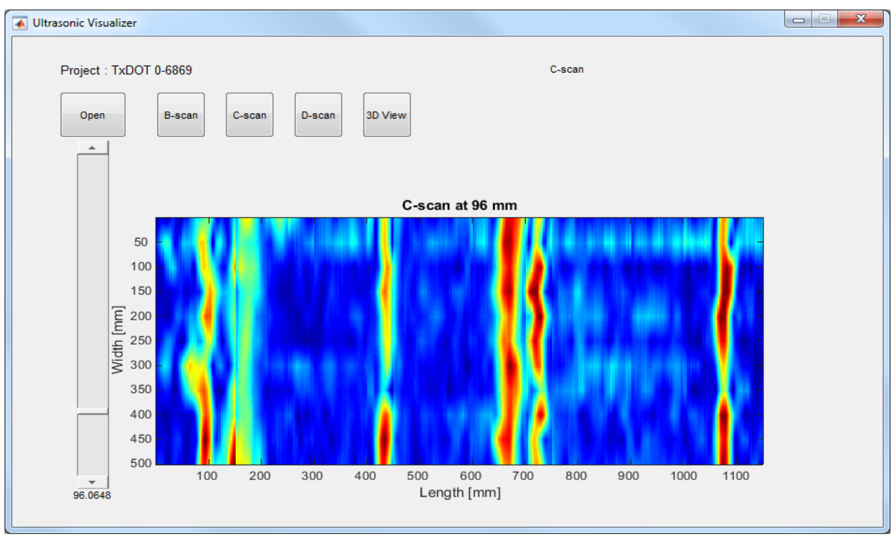 Figure 10: C-Scan of Complete Section.

<table>
<tr>
<td></td>
<td>

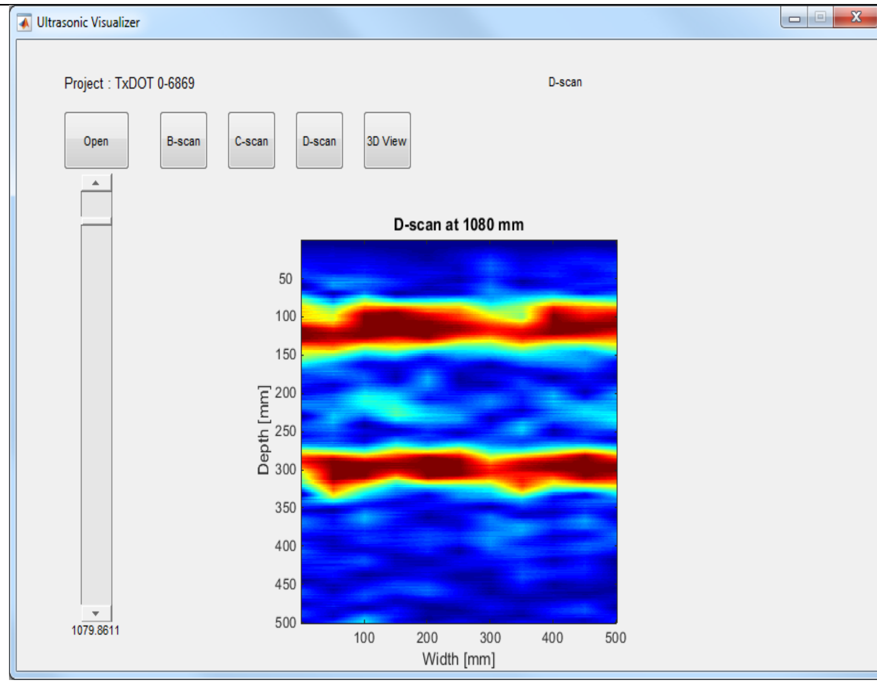

Figure 11: D-Scan of Complete Section.

REFERENCES

[1] Burr, E, Große, C., and Reinhardt, H.-W., 1998. “Application of a Modified SAFT-Algorithm on Synthetic B-scans of Coarse Grained Materials.” NDT.net, 3(2).

[2] Dengzhi, W., 2007. “Non-linear synthetic aperture focusing technology ultrasonic imaging applied in non-destructive testing.” NDT.net.

[3] Hall, T.E., Doctor, S.R. and Reig, L.D., 1986. “A Real-Time SAFT System Applied to the Ultrasonic Inspection of Nuclear Reactor Components.” *Pacific Northwest Laboratory*, Richland, WA.

[4] Kotoky, N., and Shekhar, S., 2013. “Damage Identification Using SAFT Algorithm.” *International Journal of Innovative Research in Science, Engineering and Technology,* 3(4), 194-199.

</td>
</tr>
<tr>
<td>Impacts/Benefits of Implementation (actual, not anticipated)</td>
<td>A SAFT algorithm based on time-domain was developed for this study, and it shows reliable results compared to the embedded SAFT algorithm in the MIRA device. Ultrasonic visualizer for three-dimensional and other complete sectional views (B-, C-, and D-scans) was also developed by linearly interpolating B-scans resulted from the developed algorithm. It provides a lot of intuition about defects to users.</td>
</tr>
</table>

	The work performed for this project has also resulted in a Master's Thesis listed below ➢ Williams, N. D., "Nondestructive Testing of Rail Tunnel Linings," Master's Thesis, Texas A&M University, December 2014. [(Link to PDF (30.3 MB)]
Web Links • Reports • Project website	http://www.utrgv.edu/railwaysafety/research/infrastructure/ultrasonic-tomography-for-infrastructure-inspection/index.htm